Inverse Nyquist Stability Criterion for Grid-Tied Inverters

Bo Wen, *Member, IEEE*, Dushan Boroyevich, *Fellow, IEEE*, Rolando Burgos, *Member, IEEE*, Paolo Mattavelli, *Fellow, IEEE*, and Zhiyu Shen, *Member, IEEE*

***Abstract*—A new impedance-based stability criterion was proposed for a grid-tied inverter system based on a Norton equivalent circuit of the inverter [18]. As an extension of the work in [18], this paper shows that using a Thévenin representation of the inverter can lead to the same criterion in [18]. Further, this paper shows that the criterion proposed by Middlebrook can still be used for the inverter systems. The link between the criterion in [18] and the original criterion is the inverse Nyquist stability criterion. The criterion in [18] is easier to be used. Because the current feedback controller and the phase-locked loop of the inverter introduce poles at the origin and right-half plane to the output impedance of the inverter. These poles do not appear in the minor loop gain defined in [18] but in the minor loop gain defined by Middlebrook. Experimental systems are used to verify the proposed analysis.**

***Index Terms*—Impedance, inverters, Nyquist stability, power system stability, stability.**

I. Introduction

SMALL-SIGNAL stability is of great concern for electrical power systems. Among many techniques for stability analysis, such as the eigenvalues analysis based on the system state-space model [1], the loop gain [2]–[4], and passivity [5], [6] based analysis, the impedance-based method [7]–[18] has turned out to be a very effective tool. It has been used in many applications, ranging from filter-converter systems [7], and interconnected dc–dc [8]–[10], and ac–ac [11]–[14] systems to the subsynchronous [15]–[17] and harmonic stability [18], [19] problems of grid-tied inverter systems.

Sun [18] proposed that the minor loop gain has to be computed in a certain way for predicting correctly the stability in a grid-tied inverter system: the numerator has to be the internal impedance of a voltage source (the grid), and the denominator is the internal impedance of a subsystem containing a current sink or source (the inverter) [18]–[20]. This criterion works very well for the grid-tied inverter systems.

Manuscript received May 19, 2015; revised August 30, 2015, November 5, 2015, and February 1, 2016; accepted March 8, 2016. Date of publication March 23, 2016; date of current version November 11, 2016. This work was supported by the Center for Power Electronics Systems Renewable Energy and Nanogrids miniconsortium. Recommended for publication by Associate Editor C. N. M. Ho.

B. Wen was with the Department Engineering, Electrical Engineering Division, University of Cambridge, Cambridge CB3 0FA, U.K., he is now with the School of Electrical and Electronic Engineering, University of Manchester, Manchester, M13 9PL, U.K. (e-mail: bw370@cam.ac.uk).

D. Boroyevich, R. Burgos, and Z. Shen are with the Center for Power Electronics Systems, Bradley Department of Electrical and Computer Engineering, Virginia Tech, Blacksburg, VA 24061 USA (e-mail: dushan@vt.edu; rolando@vt.edu; shenzy@vt.edu).

P. Mattavelli is with the University of Padova, Vicenza 36100, Italy (e-mail: paolo.mattavelli@unipd.it).

Color versions of one or more of the figures in this paper are available online at http://ieeexplore.ieee.org.

Digital Object Identifier 10.1109/TPEL.2016.2545871

As an extension of the work in [18], this paper gives an impedance-based small-signal stability analysis of a current-source system using the Thévenin equivalent circuit of the current source. The Thévenin equivalent circuit-based analysis leads to the same stability criterion proposed by [18]. Moreover, this paper identifies that the criterion proposed by [18] is equivalent to apply the inverse Nyquist stability criterion to the minor loop gain that the numerator is the output impedance of the current source, and the denominator is the internal impedance of the voltage source. Given that the stability conditions predicted by the inverse Nyquist stability criterion are identical to the stability conditions predicted by the Nyquist stability criterion applied to the same minor loop gain, this paper shows that the original impedance-based stability criterion proposed by [7] gives the same stability judgement as the one given by applying the criterion in [18].

For a three-phase grid-tied inverter system, a mathematic derivation in a multiple-input multiple-output (MIMO) system frame proves the equivalence of using the Thévenin and Norton equivalent circuits for stability analysis of such a system when the inverter is treated as the source. This paper concludes that when the minor loop-gain matrix is defined as the ratio between the inverter output impedance and the grid equivalent impedance matrices, it is easier to perform stability analysis by applying the generalized inverse Nyquist stability criterion (GINC) (essentially the equivalence of the criterion in [18]) than applying generalized Nyquist stability criterion (GNC) (essentially the equivalence of the criterion in [7]). This is because of the poles at the origin and right-half plane (RHP) that belong to the inverter output impedance matrix introduced by its current controller and phase-locked loop (PLL). Furthermore, when the minor loop gain is defined as the ratio between the grid equivalent impedance and the inverter output impedance matrices, using GNC is an easier way for stability analysis as it is shown in [18], because no pole of the minor loop gain is at the origin and RHP. Experiments validate the analysis.

The rest of this paper is organized as follows: Section II gives the mathematical derivation of the stability criterion for the current-source system; Section III develops the stability analysis of the three-phase grid-tied inverter system in a MIMO system frame; Section IV shows the experimental validation; Section V is the conclusion.

II. Impedance-Based Stability Analysis of a Current-Source System

A. Impedance-Based Small-Signal Stability Analysis

The original formulation of the impedance-based analysis in [7] utilizes the Thévenin representation of the "general ac

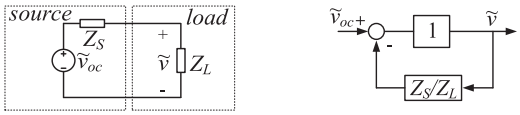

(a) (b)

Fig. 1. (a) Voltage source system with load. (b) Feedback control system.

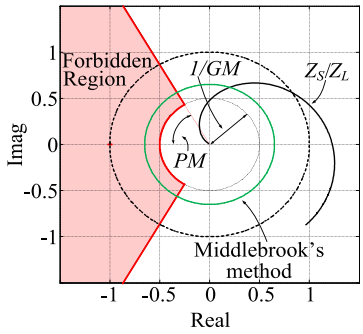

Fig. 2. Polar plot of a minor loop gain.

equivalent circuit" [7] of a voltage source with its output impedance (a filter) connected to a converter system [see Fig. 1(a)]. The source and load are designed stably with an ideal load and an ideal source respectively. Inspired by the similarity between the filter-converter system and the feedback control system [see Fig. 1(b)], the Nyquist stability criterion can be applied to the "minor loop gain" defined by the impedances ratio between the source and load (Z_S/Z_L) for stability assessment as it is applied to the loop gain of the feedback control system.

Note that the Nyquist stability criterion requires the number of the counterclockwise encirclements of the $(-1+j0)$ point by the open-loop transfer function locus be equal to the number of the RHP poles of the minor loop gain. However, in practice, the system stability is usually judged only by checking whether the locus encircles the $(-1+j0)$ point. For example, in addition to the Nyquist stability criterion, Middlebrook [7] also reported a "sufficient but more-than-necessary condition for the system stability that $|T_1| = |Z_S/Z_L| << 1$." This additional criterion is usually called Middlebrook's method (see Fig. 2). Later on, a forbidden region concept is proposed based on the desired phase margin (PM) and gain margin (GM) on the complex plane, as shown in Fig. 2, out of which the minor loop gain shall stay [8], [9]. Both the Middlebrook's method and the forbidden region concepts only consider whether the locus encircles the $(-1+j0)$ point. This is because there is no RHP pole in Z_S/Z_L for the systems discussed in [7]–[9] if the subsystems are stable individually. The criterion becomes simple without considering the RHP poles and it is still effective in practice for engineers.

However, as it has been pointed out by [18], there is "a conceptual problem when one tries to apply the existing impedance-based stability criterion to a grid-connected inverter system, as either the inverter or the grid could be treated as the source in the analysis, resulting in completely opposite stability conclusions." This problem is actually caused by ignoring the system RHP poles as identified in this paper.

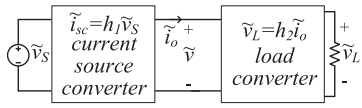

Fig. 3. Cascaded current-source converter system.

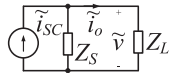

Fig. 4. Norton equivalent circuit of the system.

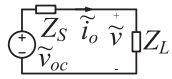

Fig. 5. Thévenin equivalent circuit of the system.

B. Current-Source System

Fig. 3 shows a current-source cascaded converter system. The current-source converter may be characterized by its input to output transfer function $h_1(s)$ without the load effect (unterminated model). The load converter is characterized by its input to output transfer function $h_2(s)$ with the resistor load.

The transfer function for the overall system is

$$h(s) = \frac{\tilde{v}_L(s)}{\tilde{v}_S(s)}. \tag{1}$$

This transfer function is important because it describes the overall system boundary-input boundary-output stability. The source can be replaced using its Norton equivalent circuit, as shown in Fig. 4.

From Figs. 3 and Fig. 4, the following relationships can be found:

$$\tilde{i}_{SC}(s) = h_1(s) \cdot \tilde{v}_S(s) \tag{2}$$

$$\tilde{v}(s) = Z_L(s) \cdot \tilde{i}_o(s) \tag{3}$$

$$\tilde{v}_L(s) = h_2(s) \cdot \tilde{i}_o(s) \tag{4}$$

$$\tilde{i}_o(s) = \tilde{i}_{SC}(s) - \frac{\tilde{v}(s)}{Z_S(s)}. \tag{5}$$

The overall input to output transfer function of the system is

$$h(s) = \frac{\tilde{v}_L(s)}{\tilde{v}_S(s)} = h_1(s) \cdot h_2(s) \frac{1}{1 + Z_L(s)/Z_S(s)}. \tag{6}$$

If the source and load are designed to be stable individually, $h_1(s)$ and $h_2(s)$ have no RHP pole, and the system stability can be judged by applying the Nyquist stability criterion to $Z_L(s)/Z_S(s)$. This is equivalent to the criterion proposed by [18].

Thévenin and Norton equivalent circuits are exchangeable in linear circuit network analysis. When a Thévenin equivalent circuit for the current-source converter is used, as shown in Fig. 5, the following relations hold:

$$\tilde{v}_{OC}(s) = Z_S(s) \cdot \tilde{i}_{SC}(s) = Z_S(s) \cdot h_1(s) \cdot \tilde{v}_S(s). \tag{7}$$

TABLE I
RELATIONSHIP BETWEEN STABILITY TEST $Z_L(s)/Z_S(s)$ AND $Z_S(s)/Z_L(s)$

Apply Nyquist to $Z_L(s)/Z_S(s)$	=	Apply inverse Nyquist to $Z_L(s)/Z_S(s)$	=	Apply Nyquist to $Z_S(s)/Z_L(s)$
j Plot locus of $Z_L(s)/Z_S(s)$		j Plot locus of $1/[Z_L(s)/Z_S(s)]$	is	j Plot locus of $Z_S(s)/Z_L(s)$
k Check RHP poles of $Z_L(s)/Z_S(s)$		k Check RHP poles of $1/[Z_L(s)/Z_S(s)]$	is	k Check RHP poles of $Z_S(s)/Z_L(s)$

Then

$$\tilde{i}_o(s) = \frac{1}{Z_S(s) + Z_L(s)} \tilde{v}_{OC}(s) \tag{8}$$

$$h(s) = \frac{\tilde{v}_L(s)}{\tilde{v}_S(s)} = h_1(s) \cdot h_2(s) \frac{1}{1 + Z_L(s)/Z_S(s)}. \tag{9}$$

The criterion that is obtained from (9) is the same as the one developed using the Norton equivalent circuit [18]. System stability can be judged by applying the Nyquist stability criterion to $Z_L(s)/Z_S(s)$.

The stability of the feedback control system with open-loop transfer function $Z_L(s)/Z_S(s)$ can also be assessed by the Nyquist stability criterion applied to the inverse plots [21], which can be considered as the inverse Nyquist stability criterion. It can be stated as follows:

"For a closed-loop system to be stable, the encirclement, if any, of the $(-1 + j0)$ point by the $1/[Z_L(s)/Z_S(s)]$ locus (as s moves along the Nyquist path) must be counterclockwise, and the number of such encirclements must be equal to the number of poles of $1/[Z_L(s)/Z_S(s)]$, that is the zeros of $Z_L(s)/Z_S(s)$, that lie on the RHP."

Note that the relationships in Table I holds. So, applying the Nyquist stability criterion to $Z_L(s)/Z_S(s)$ is equal to applying the inverse Nyquist stability criterion to $Z_L(s)/Z_S(s)$ and applying the Nyquist stability criterion to $Z_S(s)/Z_L(s)$, vice versa. However, the shapes of the Nyquist plots yielded by the two criteria could be very different.

III. IMPEDANCE-BASED STABILITY ANALYSIS OF THE GRID-TIED INVERTER SYSTEM

A. Stability Analysis

Consider the three-phase grid-tied inverter (VSI) system shown in Fig. 6. The inverter is fed by a fixed dc voltage, and connected to the grid via a three-phase inductor. The inductor currents are collected by the digital controller for feed-back control in synchronous reference frame (SRF, *dq* frame). The voltages at the point–of-common coupling (PCC) are collected by the SRF PLL [17] to synchronize the inductor currents with the PCC voltages. The small-signal analysis of a three-phase ac system is usually carried out in the *dq* frame due to the lack of an equilibrium point in the stationary frame. By performing a transformation from the stationary frame to the *dq* frame [12], [14], a balanced three-phase ac system becomes two coupled dc systems. The small-signal impedances in the *dq* frame can then be derived by performing traditional linearization [11]–[15].

Note that in the *dq* frame, the voltage and current in the system are 2-D vectors, the source and load impedances are 2×2 matrices, due to the coupling between the *d*-axis and *q*-axis,

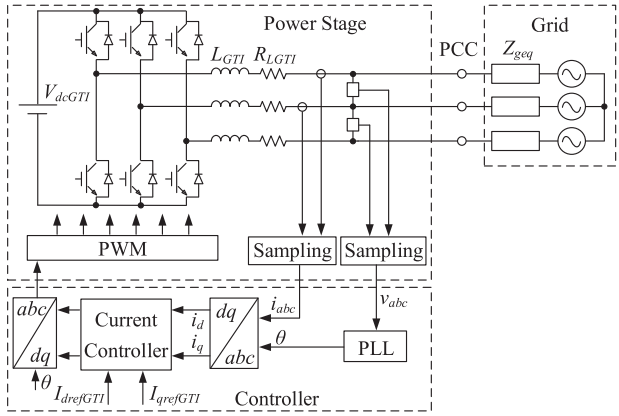

Fig. 6. Three-phase grid-tied inverter system.

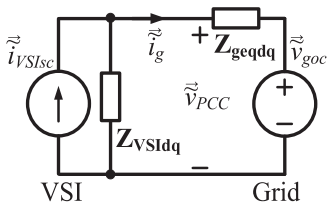

Fig. 7. Norton equivalent circuit of the grid-tied inverter system.

as

$$\mathbf{Z_{dq}}(s) = \begin{bmatrix} Z_{\mathrm{dd}}(s) & Z_{\mathrm{dq}}(s) \\ Z_{\mathrm{qd}}(s) & Z_{\mathrm{qq}}(s) \end{bmatrix}. \tag{10}$$

In the *dq* frame, the small-signal model of the inverter system that is shown in Fig. 6 can be represented using a Norton equivalent circuit for the inverter and a Thévenin equivalent circuit for the grid, as shown in Fig. 7

$$\begin{aligned} \vec{\tilde{v}}_{\mathrm{PCC}}(s) &= \left(Z^{-1}_{\mathbf{VSI}dq}(s) + \mathbf{Z^{-1}_{geqdq}}(s)\right)^{-1} \cdot \vec{\tilde{i}}_{\mathrm{VSI}sc}(s) \\ &\quad + \mathbf{Z_{VSIdq}}(s) \cdot \left(\mathbf{Z_{VSIdq}}(s) + \mathbf{Z_{geqdq}}(s)\right)^{-1} \cdot \vec{\tilde{v}}_{\mathrm{goc}}(s) \\ &= \left(\mathbf{I} + \mathbf{Z_{VSIdq}}(s) \cdot \mathbf{Z^{-1}_{geqdq}}(s)\right)^{-1} \cdot \mathbf{Z_{VSIdq}}(s) \cdot \vec{\tilde{i}}_{\mathrm{VSI}sc}(s) \\ &\quad + \left(\mathbf{I} + \mathbf{Z_{geqdq}}(s) \cdot \mathbf{Z^{-1}_{VSIdq}}(s)\right)^{-1} \cdot \vec{\tilde{v}}_{\mathrm{goc}}(s) \end{aligned} \tag{11}$$

$$\mathbf{L_{dq1}}(s) = \mathbf{Z_{VSIdq}}(s) \cdot \mathbf{Z^{-1}_{geqdq}}(s) \tag{12}$$

$$\mathbf{L_{dq2}}(s) = \mathbf{Z_{geqdq}}(s) \cdot \mathbf{Z^{-1}_{VSIdq}}(s). \tag{13}$$

From Fig. 7, (11) can be derived, it gives the expression of the PCC voltage in terms of the inverter equivalent current source, the grid equivalent voltage, and their impedances. The stability of the PCC voltage can be judged by (11). As long as the grid is

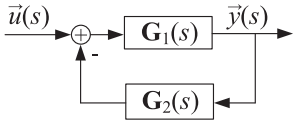

Fig. 8. Generic MIMO closed-loop configuration.

designed to be stable with an ideal load and the inverter is stable with an ideal grid, the stability of the interconnected system relies on $\mathbf{L_{dq1}}(s)$ and $\mathbf{L_{dq2}}(s)$. Hence, the PCC voltage stability at the ac interface in Fig. 7 can be studied by applying the GNC [11]–[14] or the GINC [12], [23] to the minor loop-gain matrices shown in (12) and (13), respectively

$$\vec{y}(s) = \left[\mathbf{I} + \mathbf{G}_1(s)\mathbf{G}_2(s)\right]^{-1} \mathbf{G_1}(s)\vec{u}(s) \tag{14}$$

$$\mathbf{L}(s) = \mathbf{G_1}(s)\mathbf{G_2}(s). \tag{15}$$

Let $\{l_1(s), l_2(s), \ldots, l_m(s)\}$ be the set of frequency-dependent eigenvalues of $\mathbf{L}(s)$, which trace in the complex plane the characteristic loci of matrix $\mathbf{L}(s)$ as the variable s traverses the standard Nyquist contour in the clockwise direction. Then the GNC can be formulated as follows [12], [13]:

"Let the multivariable system shown in Fig. 8 have no open-loop unobservable or uncontrollable modes whose corresponding characteristic frequencies lie in the RHP. Then, the system will be closed-loop stable if and only if the net sum of anticlockwise encirclements of the critical point $(-1 + j0)$ by the set of characteristic loci of $\mathbf{L}(s)$ is equal to the total number of RHP poles of $\mathbf{G_1}(s)$ and $\mathbf{G_2}(s)$."

The GINC [12], [23] can be formulated as:

"Let the multivariable system shown in Fig. 8 have no open-loop unobservable or uncontrollable modes whose corresponding characteristic frequencies lie in the RHP, then the system will be closed-loop stable if and only if the net sum of anticlockwise encirclements of the critical point $(-1 + j0)$ by the set of inverse characteristic loci (the reciprocal of each of the numbers $\{l_1(s), l_2(s), \ldots, l_m(s)\}$ in the complex plane) of $\mathbf{L}(s)$ is equal to the total number of RHP zeros of $\mathbf{G_1}(s)$ and $\mathbf{G_2}(s)$."

Note that $\mathbf{L_{dq2}}$ is the inverse matrix of $\mathbf{L_{dq1}}$. Thus, the eigenvalues of $\mathbf{L_{dq2}}$ are the reciprocals of the eigenvalues of $\mathbf{L_{dq1}}$ [24]. Since the poles of $\mathbf{Z_{geqdq}}$ are equal to the zeros of $\mathbf{Z_{geqdq}^{-1}}$, and the same for $\mathbf{Z_{VSIdq}^{-1}}$[24], then the system stability condition tested by applying the GNC or GINC to $\mathbf{L_{dq2}}$ is the same condition by applying the GINC or GNC to $\mathbf{L_{dq1}}$. Therefore, the stability tests that use $\mathbf{L_{dq2}}$ and $\mathbf{L_{dq1}}$ are equivalent

$$\begin{aligned}\vec{\tilde{v}}_{\mathrm{PCC}}(s) &= \mathbf{Z_{geqdq}}(s)\cdot\left(\mathbf{Z_{VSIdq}}(s)+\mathbf{Z_{geqdq}}(s)\right)^{-1}\\ &\quad\cdot\vec{\tilde{v}}_{\mathrm{VSI}oc}(s)\\ &\quad+\mathbf{Z_{VSIdq}}(s)\cdot\left(\mathbf{Z_{VSIdq}}(s)+\mathbf{Z_{geqdq}}(s)\right)^{-1}\cdot\vec{\tilde{v}}_{\mathrm{goc}}(s)\\ &= \left(\mathbf{I}+\mathbf{Z_{VSIdq}}(s)\cdot\mathbf{Z_{geqdq}^{-1}}(s)\right)^{-1}\cdot\vec{\tilde{v}}_{\mathrm{VSI}oc}(s)\\ &\quad+\left(\mathbf{I}+\mathbf{Z_{geqdq}}(s)\cdot\mathbf{Z_{VSIdq}^{-1}}(s)\right)^{-1}\cdot\vec{\tilde{v}}_{\mathrm{goc}}(s).\end{aligned} \tag{16}$$

Fig. 9 shows a Thévenin equivalent circuit of the inverter system, and the PCC voltage is (16). Recall

$$\vec{\tilde{v}}_{\mathrm{VSIoc}}(s) = \mathbf{Z_{VSIdq}}(s)\cdot\vec{\tilde{i}}_{\mathrm{VSIsc}}(s). \tag{17}$$

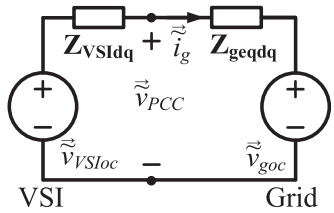

Fig. 9. Thévenin equivalent circuit of the grid-tied inverter system.

Then, (16) is the same as (11), and the minor loop-gain matrices $\mathbf{L_{dq1}}$ and $\mathbf{L_{dq2}}$ can be derived using the Thévenin equivalent circuit of the inverter system.

The analysis shown above proves that both Thévenin and Norton equivalent circuits can be used for the small-signal stability analysis of the grid-tied inverter system.

When the grid current is chosen for analysis, from both Figs. 7 and Fig. 9, the following can be derived:

$$\begin{aligned}\vec{\tilde{i}}_g(s) &= \left(\mathbf{Z_{VSIdq}}(s)+\mathbf{Z_{geqdq}}(s)\right)^{-1}\cdot\left(\vec{\tilde{v}}_{\mathrm{VSIoc}}(s)-\vec{\tilde{v}}_{\mathrm{goc}}(s)\right)\\ &= \left(\mathbf{I}+\mathbf{Z_{VSIdq}^{-1}}(s)\cdot\mathbf{Z_{geqdq}}(s)\right)^{-1}\\ &\quad\left(\vec{\tilde{i}}_{\mathrm{VSIsc}}(s)-\mathbf{Z_{VSIdq}^{-1}}(s)\,\vec{\tilde{v}}_{\mathrm{goc}}(s)\right)\end{aligned} \tag{18}$$

$$\mathbf{L_{dq3}}(s) = \mathbf{Z_{VSIdq}^{-1}}(s)\cdot\mathbf{Z_{geqdq}}(s). \tag{19}$$

System stability can be determined by applying the GNC or GINC to the minor loop-gain $\mathbf{L_{dq3}}$. Since the eigenvalues of $\mathbf{L_{dq2}}$ are the eigenvalues of $\mathbf{L_{dq3}}$, the poles and zeros of $\mathbf{L_{dq3}}$ are the poles and zeros of $\mathbf{L_{dq2}}$ [24]; therefore, the stability tests that use $\mathbf{L_{dq3}}$ and $\mathbf{L_{dq2}}$ are identical.

B. Poles of $\mathbf{Z_{VSIdq}}$

Although the stability tests using $\mathbf{L_{dq1}}$ and $\mathbf{L_{dq2}}$ are equivalent, the characteristic loci of $\mathbf{L_{dq1}}$ are the reciprocal of the characteristic loci of $\mathbf{L_{dq2}}$. The shapes of the characteristic loci of $\mathbf{L_{dq1}}$ and $\mathbf{L_{dq2}}$ could be very different. Since an inverter is designed to be stable with an ideal grid, then $\mathbf{Z_{VSIdq}^{-1}}(s)$ should have no pole on the RHP. However, $\mathbf{Z_{VSIdq}^{-1}}(s)$ could have zeros on the RHP; the zeros of $\mathbf{Z_{VSIdq}^{-1}}(s)$ are the poles of $\mathbf{Z_{VSIdq}}(s)$. When applying the GNC to $\mathbf{L_{dq1}}$, the number of counterclockwise encirclements of the $(-1 + j0)$ point by the characteristic loci should be compared with the number of the RHP pole to make the stability judgment. It is important to understand the poles of $\mathbf{Z_{VSIdq}}(s)$ when the test of applying GNC to $\mathbf{L_{dq1}}$ is used. This section provides an analysis of this issue.

The modeling of $\mathbf{Z_{VSIdq}}(s)$ consists of modeling the power stage, the current feedback control, and the PLL shown in Fig. 6. What follows briefly describes the features of $\mathbf{Z_{VSIdq}}(s)$, but the reader is referred to [25] for a detailed explanation.

The small-signal model of the three-phase grid-tied inverter is shown in Fig. 10 [25]. In Fig. 10, $\mathbf{G_{id}}$is the transfer function matrix from the duty ratio vector $\vec{\tilde{d}}^s$ to the inductor current vector $\vec{\tilde{i}}_L^s$, $\mathbf{Z_{out}}$ is the output impedance of the power stage. $\mathbf{G_{PLL}^d}$is the transfer function matrix from the system voltage $\vec{\tilde{v}}^s$to the controller dq frame duty ratio vector; $\mathbf{G_{PLL}^i}$is

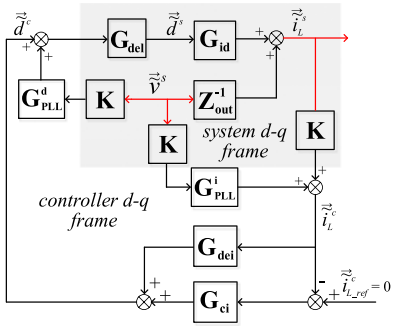

Fig. 10. Inverter small-signal model [25].

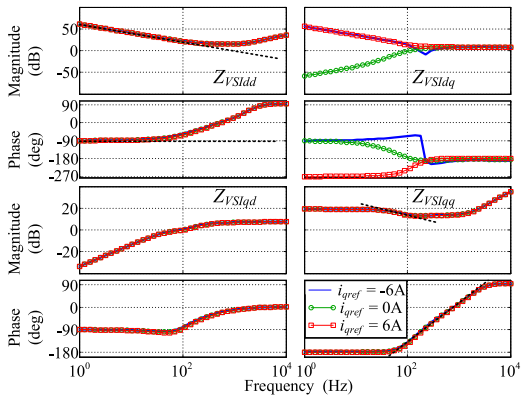

Fig. 11. Grid-tied inverter output impedances.

the transfer function matrix from the system voltage $\vec{v}^s$to the controller *dq* frame current vector $\vec{i}^c$. $\mathbf{K}$ is the transfer function matrix for voltage and current presampling filter. $\mathbf{G_{del}}$ represents the system time delay (1.5 times of the switching period) due to digital control and pulse width modulation.

Using the small-signal model shown in Fig. 10 [25] and the parameters in the Table I of [25], the impedances of a grid-tied inverter are shown in Fig. 11. Three cases are shown: the blue line shows the impedance of the capacitive power injection case; the green line shows the impedance of no reactive power injection, and the red line shows the inductive power injection case. Note that the reactive power injection will increase Z_{VSIdq}; the rest of the impedances are similar to the unit power factor case. Bode plot of Z_{VSIdd} indicates that it has a pole at the origin. This pole gives a 20dB/dec decrease of magnitude and $-90°$ phase. The bigger the current controller integral gain is, the bigger the magnitude of Z_{VSIdd} is. The Bode plot of Z_{VSIqq} shows that Z_{VSIqq} has a RHP pole. This pole causes the magnitude to decrease while the phase increases in the low-frequency range. When the bandwidth of the PLL increases, the frequency of the pole increases. When the current rating of the inverter changes, the frequency of this RHP pole changes. These features of Z_{VSIdd} and Z_{VSIqq} do not change when the grid-tied inverter injects reactive power to the grid.

In order to show the pole of Z_{VSIdd} analytically, a simplified small-signal model of the grid-tied inverter with the inductor current feedback control is given in Fig. 12. Fig. 12(a) gives a circuit diagram version of the small-signal model, while Fig. 12(b) gives a transfer function flowchart version of the

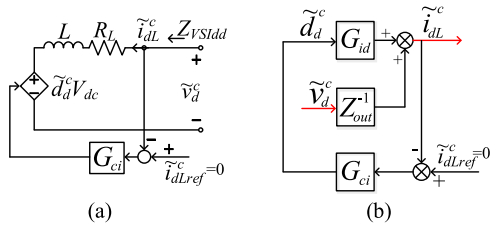

Fig. 12. *d*-channel small-signal model of the grid-tied inverter system.

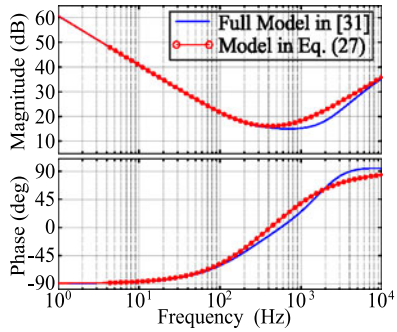

Fig. 13. Comparison between the simplified and full models for Z_{VSIdd}.

small-signal model. Compare with the full model in [25], this model neglects the effects of cross coupling, sensor dynamics, PLL, and the system delay.

In Fig. 12(b), G_{id} is the transfer function from the *d*-channel duty ratio $\tilde{d}_d^c$ to the *d*-channel inductor current $\tilde{i}_{dL}^c$; Z_{out} is the output impedance of the power stage. G_{ci} is the *d*-channel current controller

$$G_{id}(s) = -\frac{V_{\mathrm{dc}}}{Ls + R_L} \tag{20}$$

$$Z_{\mathrm{out}}(s) = Ls + R_L \tag{21}$$

$$G_{\mathrm{ci}}(s) = -\left(k_{\mathrm{pi}} + \frac{k_{\mathrm{ii}}}{s}\right). \tag{22}$$

From the simplified model shown in Fig. 12, the *d*-channel impedance of the grid-tied inverter with current feedback controller can be derived as

$$Z_{\mathrm{VSIdd\_}s}(s) = \frac{1 + G_{id} \cdot G_{\mathrm{ci}}}{Z_{\mathrm{out}}^{-1}} = \frac{Ls^2 + (R_L + V_{\mathrm{dc}}k_{\mathrm{pi}})s + V_{\mathrm{dc}}k_{\mathrm{ii}}}{s}. \tag{23}$$

Comparing the results from (23) with the results from the full model in [25] (see Fig. 13), (23) can fully represent the full model very well in the low frequency. This simplified expression of Z_{VSIdd} analytically explains that there is a pole at the origin in Z_{VSIdd}.

In order to shows the RHP pole of Z_{VSIqq} analytically, a simplified model of Z_{VSIqq} is shown in Fig. 14. As discussed in [25], because of the PLL, the inverter system has two *dq* frames: one is the system *dq* frame, and another is the controller *dq* frame. The controller *dq* frame is defined by the PLL, which estimates the position of the system *dq* frame. Due to the PLL and its dynamics, the small-signal perturbations of the system voltage propagate to the PLL output angle, and further to the

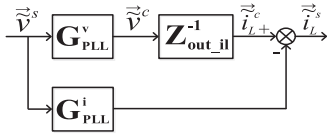

Fig. 14. q-channel small-signal model of the grid-tied inverter system.

voltage and the current in the controller dq frame. In Fig. 14, $\mathbf{G^v_{PLL}}$ (see (24) and [25]) models the small-signal perturbation path from the system voltage to the voltage in the controller dq frame. $\mathbf{G^i_{PLL}}$ (see (25) and [25]) models the small-signal perturbation path from the system voltage to the current in the controller dq frame

$$\mathbf{G^v_{PLL}} = \begin{bmatrix} 1 & V_q^s G_{\mathrm{PLL}} \\ 0 & 1 - V_d^s G_{\mathrm{PLL}} \end{bmatrix} \tag{24}$$

$$\mathbf{G^i_{PLL}} = \begin{bmatrix} 0 & I_q^s G_{\mathrm{PLL}} \\ 0 & -I_d^s G_{\mathrm{PLL}} \end{bmatrix} \tag{25}$$

$$G_{\mathrm{PLL}} = \frac{tf_{\mathrm{PLL}}}{s + V_d^s tf_{\mathrm{PLL}}} \tag{26}$$

$$tf_{\mathrm{PLL}} = k_{\mathrm{ppll}} + k_{\mathrm{ipll}} \frac{1}{s}. \tag{27}$$

In Fig. 14, $\boldsymbol{Z_{\mathrm{out\_il}}}$ is the simplified model of the output impedance matrix of the inverter with an inductor current feedback control. It ignores the Z_{dqVSI} and Z_{qdVSI}, and it also utilizes a further simplified version of (23). As discussed before, in the low frequency that within the current controller's bandwidth, Z_{VSIdd} of the inverter is mainly shaped by the integrator of the current controller. Since the PLL bandwidth is typically designed far below the bandwidth of the current loop, (28) can be a good representation of the impedance considering only the effect of current feedback control

$$\mathbf{Z_{out\_il}} = \begin{bmatrix} \dfrac{V_{\mathrm{dc}} k_{\mathrm{ii}}}{s} & 0 \\ 0 & \dfrac{V_{\mathrm{dc}} k_{\mathrm{ii}}}{s} \end{bmatrix}. \tag{28}$$

Using Fig. 14, a simplified model of Z_{VSIqq} can be calculated as follows:

$$Z_{\mathrm{VSI}qq\_s} = \frac{V_{\mathrm{dc}} k_{\mathrm{ii}} \left(s^2 + V_{\mathrm{sd}} k_{\mathrm{ppll}} s + V_{\mathrm{sd}} k_{\mathrm{ipll}}\right)}{s^3 + I_d V_{\mathrm{dc}} k_{\mathrm{ii}} k_{\mathrm{ppll}} s + I_d V_{\mathrm{dc}} k_{\mathrm{ii}} k_{\mathrm{ipll}}}. \tag{29}$$

Comparing the results from (29) with the results from the full model in [25] (see Fig. 15), (29) can represent the full model very well in the low frequency. It also shows that there is a RHP pole in Z_{VSIqq}. Using (29), expression (x_1) of this pole can be calculated as follows:

$$c = I_d V_{\mathrm{dc}} k_{\mathrm{ii}} k_{\mathrm{ppll}}; \quad d = I_d V_{\mathrm{dc}} k_{\mathrm{ii}} k_{\mathrm{ipll}} \tag{30}$$

$$x_1 = \sqrt[3]{-\frac{d}{2} + \sqrt{\frac{d^2}{4} + \frac{c^3}{27}}} + \sqrt[3]{-\frac{d}{2} - \sqrt{\frac{d^2}{4} + \frac{c^3}{27}}}. \tag{31}$$

As discussed above, the conditions for the system stability can be determined by applying the GNC or GINC to $\mathbf{L_{dq1}}$ and $\mathbf{L_{dq2}}$. For $\mathbf{L_{dq2}}$, which is defined by $\mathbf{Z_{geqdq}}$ and $\mathbf{Z^{-1}_{VSIdq}}$, it is easier to test stability by applying GNC rather than GINC. This is because there is no pole from $\mathbf{Z_{geqdq}}$ located on the RHP (otherwise, the grid would be unstable at this equilibrium point without connecting to the inverter), nor for $\mathbf{Z^{-1}_{VSIdq}}$, since all the poles of $\mathbf{Z_{VSIdq}}$ will become zeros of $\mathbf{Z^{-1}_{VSIdq}}$ [23]. Of course, if $\mathbf{Z_{VSIdq}}$ has any RHP zero, it will become the RHP pole of $\mathbf{Z^{-1}_{VSIdq}}$. However, there is no such zero in $\mathbf{Z_{VSIdq}}$, because the inverter is stable with an ideal grid. To judge the stability of the system, one can simply find whether the eigenvalue loci of $\mathbf{L_{dq2}}$ encircles the critical point $(-1 + j0)$.

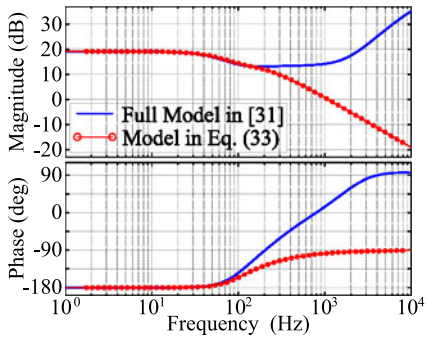

Fig. 15. Comparison between the simplified and full models for Z_{VSIqq}.

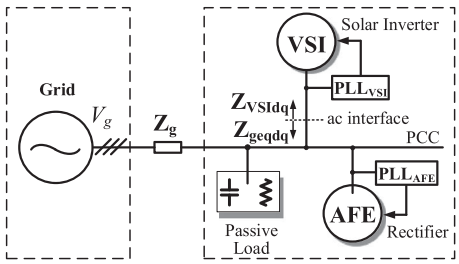

Fig. 16. Grid-tied inverter connecting to a distribution system.

For $\mathbf{L_{dq1}}$, which is defined by $\mathbf{Z_{VSIdq}}$ and $\mathbf{Z^{-1}_{geqdq}}$, it is easier to test the system stability by applying the GINC rather than the GNC. Since, although, there is no pole from $\mathbf{Z^{-1}_{geqdq}}$ located on the RHP, $\mathbf{Z_{VSIdq}}$ has one pole at the origin and one pole on the RHP, as discussed above. The standard contour for s must avoid the pole at origin, which makes the eigenvalue loci close through infinity. On the other hand, because of the RHP pole, one has to count the number of counterclockwise encirclements of the $(-1 + j0)$ point by the eigenvalue loci. All these features make the use of the GNC on $\mathbf{L_{dq1}}$ difficult. Note that when there is no RHP zero in the system, the stability condition of the system can be judged simply by checking whether the inverse characteristic loci of $\mathbf{L_{dq1}}$ encircles the critical point $(-1 + j0)$. Recall that the inverse characteristic loci of $\mathbf{L_{dq1}}$ are the reciprocal of eigenvalue loci of $\mathbf{L_{dq1}}$, which are also the characteristic loci of $\mathbf{L_{dq2}}$ since $\mathbf{L_{dq1}}$ is the inverse matrix of $\mathbf{L_{dq2}}$. Due to the pole at the origin, the inverse characteristic loci of $\mathbf{L_{dq1}}$ will concentrate around the origin which is more convenient for visual inspection.

IV. Experimental Results

A. Time-Domain Experiments

For the experimental validation, the three-phase system shown in Fig. 16 is chosen. This system is reported to have instability problem due to the designs of PLLs in the VSI and

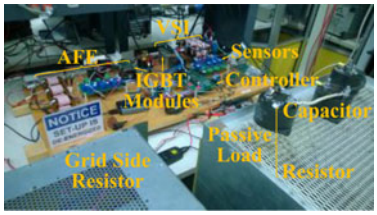

Fig. 17. Test-bed hardware prototype for an experimental system.

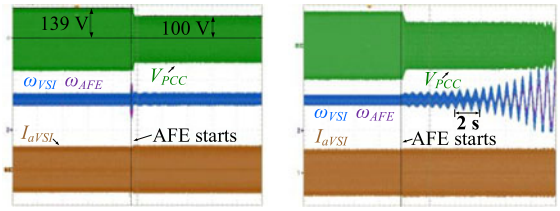

(a) (b)

Fig. 18. Experimental test results: (a) Stable case; (b) unstable case. V_{PCC} [100 V/DIV], $I_{a\mathrm{VSI}}$ [10 A/DIV], $\omega_{\mathrm{VSI}}, \omega_{\mathrm{AFE}}$ [0.05 Hz/DIV].

active front end (AFE) [22]. This problem is analyzed using the impedance-based criterion (applying the GNC to $\mathbf{L_{dq2}}$) proposed by [18] in [17]. This section details applying the GNC to $\mathbf{L_{dq1}}$ and the equivalence of this analysis to that shown in [17].

There are four components in the system, including a VSI, an AFE of motor drive, a passive load, and the grid. The power stage and control scheme of the VSI is the same as shown in Fig. 6. The power stage of the AFE is a two-level three-phase boost rectifier (see Section II in [17]). The PCC voltages are measured so that the PLL can perform the grid synchronization for the AFE. The boost inductor currents and output voltages are measured by inner current and outer voltage feedback control loops. All the control systems of AFE are implemented in the *dq* frame. The grid side impedance is a three-phase resistor R_g, and the passive load impedance is a three-phase parallel connected capacitor C_{Load} and resistor R_{Load}.

A low-power test-bed hardware prototype of the system shown in Fig. 16 is built in the laboratory (see Fig. 17). Its parameters can be found in the Table II of [17]. In the experiment, the VSI is started first, and then the AFE is turned on. Two experiments are performed. In the first experiment [see Fig. 18(a)], the VSI and AFE work stably with the grid and the passive load. The grid is emulated by a three-phase programmable power supply series-connected with a three-phase resistors. In the second experiment, the system is unstable [Fig. 18(b)]. Only the PLL parameters of VSI and AFE are changed between the stable to unstable tests.

B. Impedance-Based Stability Analysis Using $L_{1\mathrm{dq}}$

The grid side and the passive load impedance matrices are shown as

$$\mathbf{Z_{gdq}}(s) = \begin{bmatrix} R_g & 0 \\ 0 & R_g \end{bmatrix} \tag{32}$$

$$\mathbf{Z_{CLoaddq}}(s) = \begin{bmatrix} C_{\mathrm{Load}}s & -\omega C_{\mathrm{Load}} \\ \omega C_{\mathrm{Load}} & C_{\mathrm{Load}}s \end{bmatrix}^{-1} \tag{33}$$

$$\mathbf{Z_{RLoaddq}}(s) = \begin{bmatrix} R_{\mathrm{Load}} & 0 \\ 0 & R_{\mathrm{Load}} \end{bmatrix}. \tag{34}$$

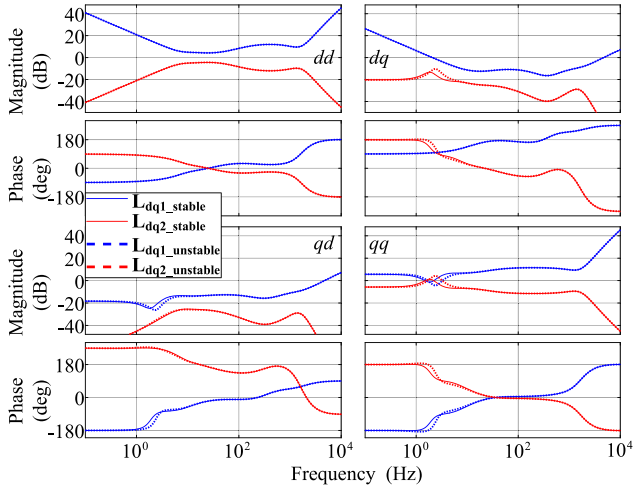

Fig. 19. $L_{1\mathrm{dq}}$ and $L_{2\mathrm{dq}}$ for stable and unstable cases.

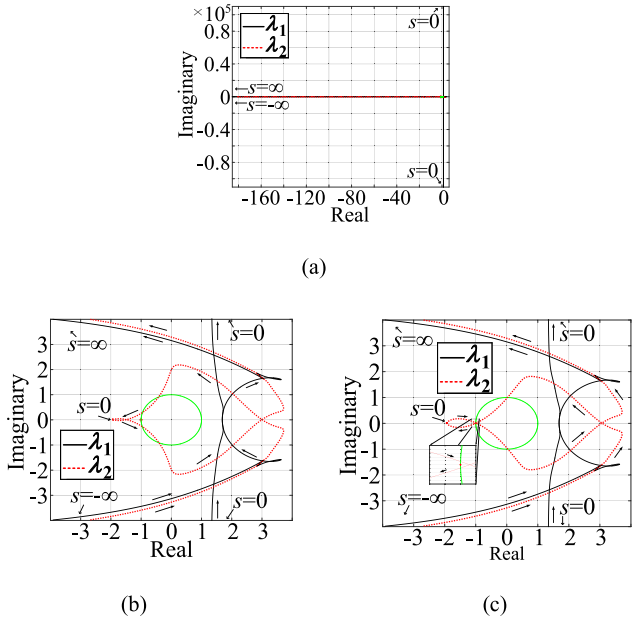

(a)

(b) (c)

Fig. 20. Characteristic loci of $L_{1\mathrm{dq}}$: (a) Zoomed-out view of stable case; (b) zoomed-in view of stable case; (c) Zoomed-in view of unstable case.

The input impedance of AFE is discussed thoroughly in [14], [15], and [26]–[28]. In this paper, the equation of $\mathbf{Z_{AFEdq}}$ is from [17]. Note that with the parameters of the experimental system, $\mathbf{Z_{CLoaddq}}$, $\mathbf{Z_{RLoaddq}}$, $\mathbf{Z_{AFEdq}}$, and $\mathbf{Z_{gdq}}$ are nonsingular. Thus, the equivalent grid-side impedance is

$$\mathbf{Z_{geqdq}}(s) = \left(\mathbf{Z}^{-1}_{\mathbf{CLoaddq}}(s) + \mathbf{Z}^{-1}_{\mathbf{RLoaddq}}(s) + \mathbf{Z}^{-1}_{\mathbf{AFEdq}}(s) + \mathbf{Z}^{-1}_{\mathbf{gdq}}(s)\right)^{-1}. \tag{35}$$

Bode plots of $\mathbf{Z_{VSIdq}}$ and $\mathbf{Z_{geqdq}}$ for the stable and unstable cases can be found in [17, Fig. 28].

$\mathbf{L_{dq1}}$ and $\mathbf{L_{dq2}}$ can be calculated for both the stable and unstable cases using $\mathbf{Z_{VSIdq}}$ and $\mathbf{Z_{geqdq}}$, as shown in Fig. 19. It can be observed that at low frequencies, the magnitudes of the *dd* and *dq* elements of $\mathbf{L_{dq1}}$ are high, and they increase when the frequency decreases. At high frequencies, the *dd* and *qq* elements of $\mathbf{L_{dq1}}$ also have high magnitudes, and they increase

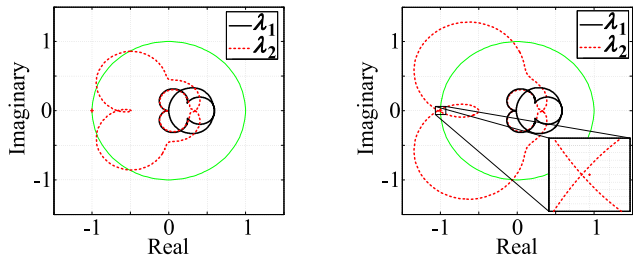

Fig. 21. Inverse characteristic loci of $\mathbf{L_{dq1}}$: (a) Stable; (b) unstable.

when the frequency increases. Then, the eigenvalues of $\mathbf{L_{dq1}}$ close through the infinity at zero frequency and high frequency. This can be seen from Fig. 20(a). Fig. 20(b) shows a zoomed-in view of the stable case. λ_2 encircles the critical point counterclockwise once. Considering there is only one RHP pole of $\mathbf{Z_{VSIdq}}$ and $\mathbf{Z_{geqdq}^{-1}}$, when the GNC is applied to $\mathbf{L_{dq1}}$, the system is stable. Fig. 20(c) shows a zoomed-in view of the unstable case. λ_2, encircles the critical point clockwise once, when the GNC is applied to $\mathbf{L_{dq1}}$, the system is unstable.

Fig. 21 shows the inverse characteristic loci of $\mathbf{L_{dq1}}$. They are also the characteristic loci of $\mathbf{L_{dq2}}$. By applying the GINC to $\mathbf{L_{dq1}}$, just as with applying the GNC to $\mathbf{L_{dq2}}$ [17], the stability condition of the experimental system can be predicted accurately by just checking whether the loci encircle the $(-1 + j0)$ point.

V. Conclusion

Impedance-based small-signal stability criterion is derived using the Thévenin representation for the current-source system. The original criterion proposed by Middlebrook can still be used for a current-source system, the poles at the origin, and the RHP must be considered. However, applying the inverse Nyquist stability criterion to the minor loop gain defined by Middlebrook is equivalent to the criterion in [18]. For the three-phase grid-tied inverter system discussed in this paper, the current feedback controller and the PLL introduce poles to its output impedance at origin and the RHP. The stability test of applying the GNC to the minor loop gain defined by the ratio of the grid impedance over the inverter impedance, or applying the GINC to the minor loop gain defined by the ratio of the inverter impedance over the grid impedance, leads to an easier stability judgment. The poles at origin and RHP of the inverter output impedance can be ignored. Stability of the system can be judged simply by checking whether the characteristic loci encircle the $(-1, j0)$ point. The above analyses show that in many new applications, the poles on the origin and RHP of the impedance of a component must be considered if there is any, because they play an important role in the impedance-based stability analysis. A three-phase experimental system validated the proposed analyses.

References

[1] N. Bottrell, M. Prodanovic, and T. C. Green, "Dynamic stability of a microgrid with an active load," *IEEE Trans. Power Electron.*, vol. 28, no. 11, pp. 5107–5119, Nov. 2013.

[2] R. D. Middlebrook, "Measurement of loop gain in feedback systems," *Int. J. Electron.*, vol. 38, no. 4, pp. 485–512, 1975.

[3] Y. Panov and M. M. Jovanovic, "Stability and dynamic performance of current-sharing control for paralleled voltage regulator modules," *IEEE Trans. Power Electron.*, vol. 17, no. 2, pp. 172–179, Mar. 2002.

[4] J. Morroni, R. Zane, and D. Maksimovic, "An online stability margin monitor for digitally controlled switched-mode power supplies," *IEEE Trans. Power Electron.*, vol. 24, no. 11, pp. 2639–2648, Nov. 2009.

[5] J. Zeng, Z. Zhe, and W. Qiao, "An interconnection and damping assignment passivity-based controller for a dc-dc boost converter with a constant power load," *IEEE Trans. Ind. Appl.*, vol. 50, no. 4, pp. 2314–2322, Jul./Aug. 2014.

[6] Y. Gu, W. Li, and X. He, "Passivity-based control of dc microgrid for self-disciplined stabilization," *IEEE Trans. Power Syst.*, vol. 30, no. 5, pp. 2613–2632, Sep. 2015.

[7] R. D. Middlebrook, "Input filter considerations in design and application switching regualtors," in *Proc. IEEE Ind. Appl. Soc. Annu. Conf.*, 1976, pp. 366–382.

[8] C. M. Wildrick, F. C. Lee, B. H. Cho, and B. Choi, "A method of defining the load impedance specification for a stable distributed power system," *IEEE Trans. Power Electron.*, vol. 10, no. 3, pp. 280–285, May 1995.

[9] X. Feng, J. Liu, and F. C. Lee, "Impedance specification for stable dc distributed power systems," *IEEE Trans. Power Electron.*, vol. 17, no. 2, pp. 157–162, Mar. 2002.

[10] H. W. Wallen and S. J. Fu, "United States laboratory element electrical power system verification approach," *J. Propulsion Power*, vol. 13, no. 4, pp. 570–573, Jul. 1997.

[11] Z. Yao, P. G. Therond, and B. Davat, "Stability analysis of power systems by the generalised Nyquist criterion," in *Proc. Int. Conf. Control*, Mar. 1994, pp. 739–744.

[12] M. Belkhayat, "Stability criteria for ac power systems with regulated loads," Ph.D. dissertation, Elect. Comput. Eng., Purdue Univ., West Lafayette, IN, USA, Dec. 1997.

[13] A. G. J. MacFarlane and I. Postlethwaite, "The generalized Nyquist stability criterion and multivariable root loci," *Int. J. Control*, vol. 25, pp. 81–127, 1977.

[14] B. Wen, D. Boroyevich, R. Burgos, P. Mattavelli, and Z. Shen, "Small-signal stability analysis of three-phase ac systems in the presence of constant power loads based on measured *d-q* frame impedances," *IEEE Trans. Power Electron.*, vol. 30, no. 10, pp. 5952–5963, Oct. 2015.

[15] L. Harnefors, M. Bongiorno, and S. Lundberg, "Input-admittance calculation and shaping for controlled voltage-source converters," *IEEE Trans. Ind. Electron.*, vol. 54, no. 6, pp. 3323–3334, Dec. 2007.

[16] K. M. Alawasa, Y. A. R. I. Mohamed, and W. Xu, "Active mitigation of subsynchronous interactions between PWM voltage-source converters and power networks," *IEEE Trans. Power Electron.*, vol. 29, no. 1, pp. 121–134, Jan. 2014.

[17] B. Wen, D. Dong, D. Boroyevich, R. Burgos, P. Mattavelli, and Z. Shen, "Impedance-based analysis of grid-synchronization stability for three-phase paralleled converters," *IEEE Trans. Power Electron.*, vol. 31, no. 1, pp. 26–38, Jan. 2016.

[18] J. Sun, "Impedance-based stability criterion for grid-connected inverters," *IEEE Trans. Power Electron.*, vol. 26, no. 11, pp. 3075–3078, Nov. 2011.

[19] X. Wang, F. Blaabjerg, and W. Wu, "Modeling and analysis of harmonic stability in an ac power-electronics-based power system," *IEEE Trans. Power Electron.*, vol. 29, no. 12, pp. 6421–6432, Dec. 2014.

[20] S. Vesti, T. Suntio, J. A. Oliver, R. Prieto, and J. A. Cobos, "Impedance-based stability and transient-performance assessment applying maximum peak criteria," *IEEE Trans. Power Electron.*, vol. 28, no. 5, pp. 2099–2014, May 2013.

[21] K. Ogata, *Modern Control Engineering*, 5th ed. Englewood Cliffs, NJ, USA: Prentice-Hall, 2010.

[22] D. Dong, B. Wen, P. Mattavelli, D. Boroyevich, and Y. Xue, "Grid-synchronization modeling and its stability analysis for multi-paralleled three-phase inverter systems," in *Proc. 28th Annu. Appl. Power Electron. Conf. Expo.*, Mar. 2013, pp. 439–446.

[23] I. Postlethwaite, "A generalizd inverse nyquist stability criterion," *Int. J. Control*, vol. 26, pp. 325–340, 1977.

[24] S. Skogestad and I. Postlethwaite, *Multivariable Feedback Control : Analysis and Design*. Hoboken, NJ, USA: Wiley, 2005.

[25] B. Wen, D. Boroyevich, R. Burgos, P. Mattavelli, and Z. Shen, "Analysis of *d-q* small-signal impedance of grid-tied inverters," *IEEE Trans. Power Electron.*, vol. 31, no. 1, pp. 675–687, Jan. 2015.

[26] M. Schweizer and J. W. Kolar, "Shifting input filter resonances—An intelligent converter behavior for maintaining system stability," in *Proc. Int. Power Electron. Conf. ECCE Asia*, May 2010, pp. 906–913.

[27] B. Wen, D. Boroyevich, P. Mattavelli, Z. Shen, and R. Burgos, "Influence of phase-locked loop on input admittance of three-phase voltage-source converters," in *Proc. 28th Annu. Appl. Power Electron. Conf. Expo.*, Mar. 2013, pp. 897–904.

[28] H. Mao, D. Boroyevich, and F. C. Lee, "Novel reduced-order small-signal model of a three-phase PWM rectifier and its application in control design and system analysis," *IEEE Trans. Power Electron.*, vol. 13, no. 3, pp. 511–521, May 1998.

Bo Wen (S'11–M'15) received the B.S. degree in electrical engineering from Xi'an Jiaotong University, Xi'an, China, in 2006, and the M.S. and Ph.D. degrees in electrical engineering from Virginia Tech, Blacksburg, VA, USA, in 2011 and 2014, respectively.

He is currently a Research Associate at the Department of Engineering, Electrical Engineering Division, University of Cambridge, Cambridge, U.K. His current research interests include multiphase power conversion, power electronics systems modeling, and stability analysis.

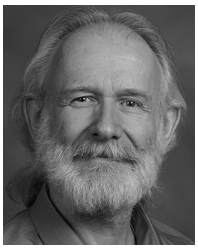

Dushan Boroyevich (S'81–M'86–SM'03–F'06) received the Dipl.Ing. degree from the University of Belgrade, Belgrade, Serbia, in 1976, the M.S. degree from the University of Novi Sad, Novi Sad, Serbia, in 1982, and the Ph.D. degree from Virginia Polytechnic Institute and State University (Virginia Tech), Blacksburg, VA, USA, in 1986.

From 1986 to 1990, he was an Assistant Professor and Director of the Power and Industrial Electronics Research Program with the Institute for Power and Electronic Engineering, University of Novi Sad, and later, acting as the Head of the Institute. He then joined the Bradley Department of Electrical and Computer Engineering, Virginia Tech, as an Associate Professor, where he is currently the American Electric Power Professor at the Department and the Codirector at the Center for Power Electronics Systems. His research interests include multiphase power conversion, electronic power distribution systems, power electronics systems modeling and control, and integrated design of power converters.

Prof. Boroyevich was the President of the IEEE Power Electronics Society from 2011 to 2012. He received the IEEE William E. Newell Power Electronics Technical Field Award, and a Member of the U.S. National Academy of Engineering.

Rolando Burgos (S'96–M'03) received the B.S. degree in electronics engineering, the Electronics Engineering Professional degree, and the M.S. and Ph.D. degrees in electrical engineering from the University of Concepción, Concepción, Chile, in 1995, 1997, 1999, and 2002, respectively.

In 2002, he joined, as a Postdoctoral Fellow, the Center for Power Electronics Systems (CPES), Virginia Tech, Blacksburg, VA, USA, where he became a Research Scientist in 2003, and a Research Assistant Professor in 2005. In 2009, he joined the ABB Corporate Research, Raleigh, NC, USA, as a Scientist, and became a Principal Scientist in 2010. In 2010, he was appointed as an Adjunct Associate Professor with the Electrical and Computer Engineering Department, North Carolina State University, working at the Future Renewable Electric Energy Delivery and Management Systems Center. In 2012, he returned to Virginia Tech, where he is currently an Associate Professor at the Bradley Department of Electrical and Computer Engineering and CPES Faculty. His research interests include multiphase multilevel power conversion, grid power electronics systems, stability of ac and dc power systems, and high-power density power electronics, modeling, and control theory and applications.

Dr. Burgos is a Member of the IEEE Power Electronics Society, where he currently serves as an Associate Editor of the IEEE TRANSACTIONS ON POWER ELECTRONICS, the IEEE POWER ELECTRONICS LETTERS, and the IEEE JOURNAL OF EMERGING AND SELECTED TOPICS IN POWER ELECTRONICS. He is also the Vice-chair of the Power and Control Core Technologies Committee of the Power Electronics Society. He is also a Member of the IEEE Industry Applications Society and of the IEEE Industrial Electronics Society.

Paolo Mattavelli (S'95–A'96–M'00–SM'10–F'14) received the M.S. (Hons.) degree and the Ph.D. degree in electrical engineering from the University of Padova, Vicenza, Italy, in 1992 and 1995, respectively.

From 1995 to 2001, he was a Researcher with the University of Padova. From 2001 to 2005, he was an Associate Professor with the University of Udine, where he led the Power Electronics Laboratory. In 2005, he joined the University of Padova with the same duties. From 2010 to 2012, he was a Professor and Member with the Center for Power Electronics Systems, Virginia Tech. Since 2016, he has been a Professor with the University of Padova. His major field of research interests include analysis, modeling, and analog and digital control of power converters, grid-connected converters for renewable energy systems and microgrids, and high-temperature and high-power density power electronics. In these research fields, he has been leading several industrial and government projects. His current google scholar h-index is 50.

Dr. Mattavelli from 2003 to 2012, served as an Associate Editor for the IEEE TRANSACTIONS ON POWER ELECTRONICS. From 2005 to 2010, he was the Industrial Power Converter Committee Technical Review Chair for the IEEE TRANSACTIONS ON INDUSTRY APPLICATIONS. For terms 2003–2006, 2006–2009, and 2013—2015, he has been a member-at-large of the IEEE Power Electronics Society's Administrative Committee. He also received the Prize Paper Award in the IEEE TRANSACTIONS ON POWER ELECTRONICS in 2005, 2006, 2011, and 2012, respectively, and in 2007, the second Prize Paper Award at the IEEE Industry Application Annual Meeting..

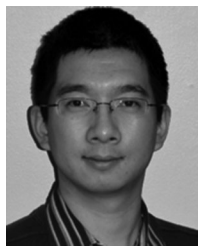

Zhiyu Shen (S'11–M'13) received the B.S. and M.S. degrees in electrical engineering from Tsinghua University, Beijing, China, in 2004 and 2007, respectively, and the Ph.D. degree in electrical engineering from Virginia Tech, Blacksburg, VA, USA, in 2013.

He is currently a Research Scientist at the Center for Power Electronics System, Virginia Tech. His research interests include three-phase ac system impedance measurement, three-phase ac system small-signal stability, high-frequency high-density converter design, and control system architecture in high-power converters.